London Journal of PHYSICS

Volume 1 No 2

Electronic Nature and Thermoelectric Characteristics of Cubic $LaPb_3$ $LaIn_3$ and $LaTl_3$ Compounds: B3PW91 Approach

Qasimullah[1], Irfan Ullah[2], Muhammad Irfan[3]

[1]Faculty of Physical and Numerical Sciences. Qurtuba University of Science and Information Technology, Peshawar 25100, Pakistan
[2]Department of Physics Abdul Wali Khan University Mardan 23200, KP, Pakistan
[3]University of Brasilia, Institute of Physics, Brasilia 70919-970, DF, Brazil

qasimullah9966@gmail.com

December 4, 2024

Abstract

In this paper the structural, electronic and transport properties of the strongly correlated intermetallics LaX_3 (X=Pb, In and Tl) in the space group Pm-3m (221) have been investigated using B3PW91 hybrid functional within the framework of density functional theory. These compounds have $4f$ orbitals and hence strong electron-electron correlation effect is expected, therefore, the electronic properties are also calculated with the B3PW91 hybrid functional and the effect of B3PW91 hybrid functional on the density of states is discussed in details. The band structure and density of states, demonstrate the metallic nature of these compounds. Using the semi-empirical Boltzmann's approach implemented in the BoltzTraP code, the transport parameters, such as the Seebeck coefficient, electrical conductivity, thermal conductivity and figure of merit as a function of the chemical potential are computed at a temperature gradient of 500 K. For all materials the thermal and electrical conductivities, and Seebeck coefficient has higher values for n-type doping in comparison with p-type doping. The moderate values of figure of merit obtained for these materials indicate that these materials have applicability where small values of thermoelectric efficiency are required and higher values can harm the process but need experimental verification. $LaIn_3$ has the highest value of electrical conductivity per relaxation time and thermal conductivity per relaxation time are 9.43 x 10^{20} 1/Ωms and 107.65 x 10^{14} W/mKs respectively. $LaTl_3$ has the highest figure of merit among these materials.

1 Introduction

Strongly correlated electronic systems include f-block elements and their compounds are more attractive in condensed-matter physics because of their numerous practical applications, properties and fascinating physics. Some materials have exceptional magnetic, electrical, optical, and mechanical properties that depend on electron-electron correlation phenomena [1-3]. The history of the correlated electronic materials began in 1930's of prior eras. Theoretical concepts were initially created before there was a lot of actual effort in this field. Wigner introduced the key ideas using the idea of an electron crystal lattice [4]. RX_3 systems (R= Rare-earth and X= Pb, In, Tl) with space group is Pm-3m (221) have been explored experimentally and theoretically by many researchers due to the phenomena of magnetism, superconductivity, crystal field effect, and kondo type behaviors. Some of these systems exhibit the coexistence of large, temperature-dependent paramagnetic susceptibility and superconducting transition temperature. The transition temperatures of $LaPb_3$ and $LaTl_3$ compounds are greater than $LaIn_3$ but $LaIn_3$ has a transition temperature of little more than 1 K. Lead atoms are in quadrivalent ionic state, but indium or thallium atoms are in a trivalent ionic state. The valences of the lanthanide in RX_3 compounds can be estimated using the lattice constant

 DOI 10.69710/ljp.v1i2.11037

measuring method. For pure lanthanides, Ln^{2+} has a nearly 10% greater lattice constant than Ln^{3+} [5-10]. Due to intriguing qualities, including large melting points, ductility, best physical properties, lanthanides based intermetallic materials are desirable materials for research. Additionally, rare-earth intermetallics are superior to other metals as materials for the development of commercial aviation turbines [11-12]. Due to the fact that RX_3 compounds crystallize in a variety of crystal forms with varying atomic coordination and bond length values, the rare-earth in several practical applications, intermetallics RX_3 exhibit outstanding physical qualities [13]. Rare-earth intermetallics put in a noteworthy performance in numerous technological applications. This is true both conceptually and practically. RX_3 (R= Rare-earth and X = Pb, In) with a cubic crystal structure are preferred for industrial applications [14-15]. RIn_3 and RSn_3 chemicals exhibit lanthanide contraction across the whole series. RX_3 compounds are easy to form in a single crystal due to their proper coherent melting. In contrast, X can be replaced by a member of group IIIA, IVA, or a transition metal to create a huge variety of RX_3 intermetallic compounds. When X is changed, these compounds may take on a broad variety of forms (X might be (In, Tl, Pb), of these compounds are straightforward to make since they melt identically. Since cubic symmetry crystallizes in many RX_3 compounds, it is preferred to lower symmetry for superconductivity and can be further boosts ductility in the aerospace industry [1619]. In this article we study the electronic and transport properties of the rare-earth LaX_3 (X=Pb, In and Tl) materials using HF B3PW91 within the frame work of DFT. Electronic properties of these materials are investigated on the basis of spin polarized electronic band structure, total and partial density of states. Transport properties of these materials are calculated at the first time.

2 Computational detail

In the last century Density functional theory (DFT) has appeared as a strong theoretical technique to investigate the physical and chemical properties of crystal materials. DFT has been a widely utilized tool in most fields of chemistry and material sciences due to its inexpensive computational cost and useful precision [20]. To solve the Kohn–Sham equations, these computations are carried out using a computer program [21]. LaX_3 (X=Pb, In, and Tl) intermetallic compounds are theoretically analyzed and their ground state characteristics are determined using the Full Potential Linearized Augmented Plane Waves (FP-LAPW) method, which is based on DFT [22–23] in the Wien2K program [24]. A useful tool for explaining highly linked electrical systems is HF. B3PW91 has the ability to effectively address these systems in lanthanides [25]. Similarly, to achieve better results in the HF computations, the precise exchange α is chosen to 0.2 eV. The plane wave basis functions are determined via RMTKmax$\frac{1}{4}$8.00 using 286 k-points. Non-shifted meshes with 1000 k points are utilized for the electronic computations, while 10000 k points are used for the transport calculation. Using the BoltzTraP code, the calculated electronic structures are utilized to examine related to thermoelectric parameters [26]. Two junctions consisting of dissimilar conductors or semiconductors are kept at different temperatures ΔT, which results in the passage of electrical current, the system under study exhibits its thermoelectric features. The Seebeck effect is what leads to the generation of this thermoelectric power. The open-circuit potential difference ΔV is defined by the equation $\Delta V = (S)\Delta T$, where "S" stands for the Seebeck coefficient, expressed in $V.K^{-1}$. $ZT = S^2T(\sigma/\kappa)$ is the formula used to compute the dimensionless thermoelectric figure of merit (ZT), which is used to evaluate a material's thermoelectric performance [27].

3 Results and discussion

3.1 Electronic Charge Density

The electronic charge density gives a thorough understanding of bulk bonding, which can be ionic or covalent, as well as the bonding characteristics of materials [28]. The electron charge density can be determined by choosing various cell planes because we are dealing with a material's properties in DFT. The two dimensional (2-D) electron charge density for LaX_3 (X=Pb, In and Tl) materials in (100) planes are presented in Figure 3.1(a,b,c). The distribution of the electronic charge density is spherical around Pb, In and Tl atoms and very small charge density in the region between the Pb, In and Tl atoms indicate that the bond between La and X atoms is ionic. Pb is bonded in a distorted square geometry to La atoms. The strong ionic connection between lanthanum/indium and lanthanum/thalium which is demonstrated in the plots, also indicates that

 DOI 10.69710/ljp.v1i2.11037

the overall bonding in these compounds is ionic. Lead makes strong ionic bond with La atom, because lead electronegativity is higher than indium and thallium.

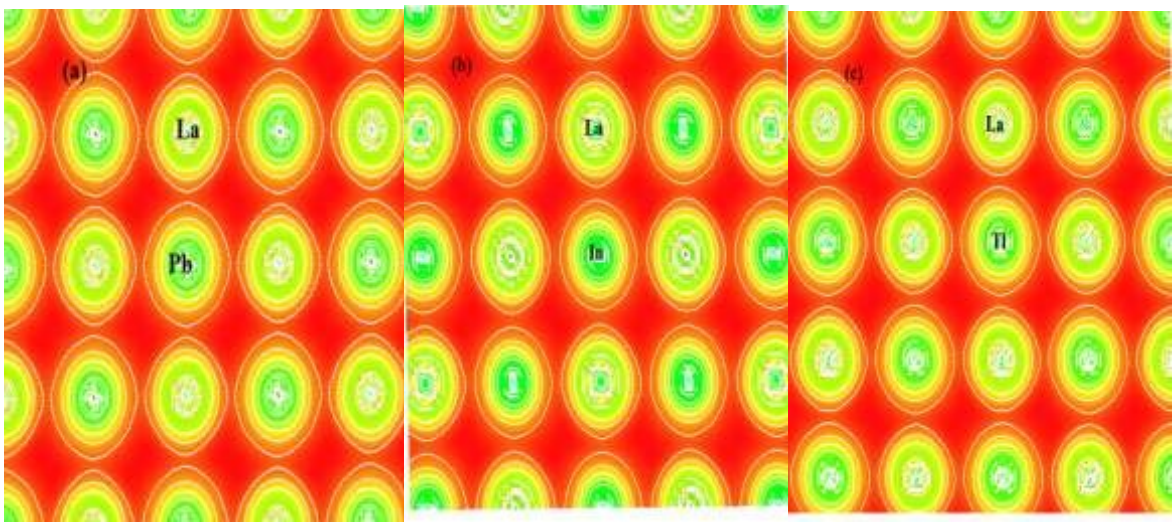

Figure 3.1(a,b,c): The electronic charge density of $LaPb_3$, $LaIn_3$ and $LaTl_3$

3.2 Band Structure

One of the most fundamental characteristics that gives a molecule its different physical properties is its band gap. Accurate measurements of physical properties, such as electrical and thermoelectric capacities, are made possible by band gaps. A material's band structure must be understood before it can be technically used in a variety of future technologies [29]. Spinning band occurs due to GGA's inability to correctly handle f-state, La f-state manifests at the Fermi level. We employ HF B3PW91 to get over this issue and localize the f-state electrons. By employing HF B3PW91, the f-state was correctly localized. In Figure 3.2(a,b,c) the energy range from -14 eV to 8 eV which is observed along the high symmetry directions in the first Brillouin zone. At zero pressure, the bands at the Fermi level for materials $LaPb_3$, $LaIn_3$, and $LaTl_3$ are extremely similar along all high symmetry lines. The different colors in the band structure represent the energy states. Which is clearly described in DOS. At 0.0 eV, the Fermi energy level between the valence band and conduction band is assumed. The Figures 3.2(a,b,c) also show that in all compounds, the symmetry point τ, X and M is where the states overlap. No bandgap is observed for these compounds, hence all of them are metallic.

 DOI 10.69710/ljp.v1i2.11037

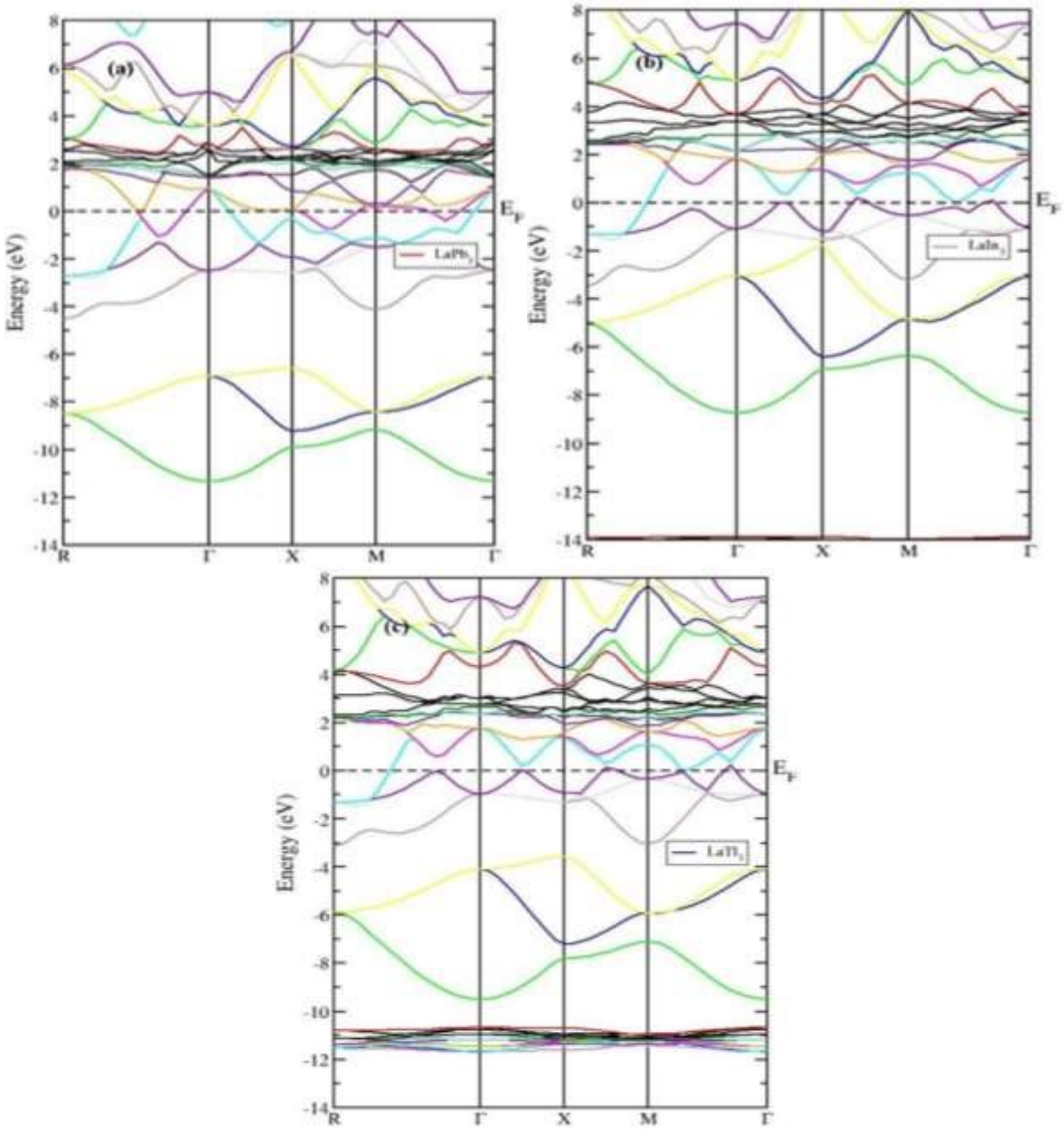

Figure 3.2(a,b,c): Band structure of $LaPb_3$, $LaIn_3$ and $LaTl_3$ for spin up calculation.

3.3 Density of States

The strongly correlated systems such as lanthanides (actinides) which involve 4f (5f) orbitals have interesting physical and chemical properties, because these electrons can be localized or itinerant depending on the crystalline environment [3]. Therefore, to understand the effects of the 4f orbitals in these compounds, the calculations are carried out using the B3PW91 hybrid functional are used to explain the effects of the 4f orbital in compounds based on rare-earth elements [30]. Figures 3.3 displays the total density of states (TDOS with the B3PW91 hybrid functional as well as the partial density of states (DOS) for $LaPb_3$, $LaIn_3$ and $LaTl_3$ materials. Density of state plots of $LaPb_3$,

$LaIn_3$, and $LaTl_3$ show that these compounds have the potential to be useful thermoelectric materials because of the strong peaks that are correlated with higher carrier concentrations close to the valence band edge. This information is taken from the partial density of states graphs shown in Figures 3.3, which allow

 DOI 10.69710/ljp.v1i2.11037

us to understand how frequently each state occurs inside the valence and conduction bands of the atom [31-33]. Figure 3.3(a,b,c) displays the results of the TDOS and PDOS computations for the $LaPb_3$, $LaIn_3$ and $LaTl_3$ materials. The range between -10 eV to 7 eV. At the Fermi level, most of the contribution comes from the f state of La, while other states make an almost negligible contribution. The use of the B3PW91 hybrid functional clearly shows that the strong peaks caused by the 4f states are greatly pushed higher. The TDOS peak observed for $LaPb_3$, $LaIn_3$ and $LaTl_3$ are 13 states/eV, 10.5 states/eV and 11.6 states/eV respectively. Among these materials, the maximum TDOS peak is observed for $LaPb_3$ which is 13 states per eV. La-f and Lad make up the majority of the contribution above E_f. States Pb-s, In-s and Tl-s below the E_f , while other states have negligible contribution.

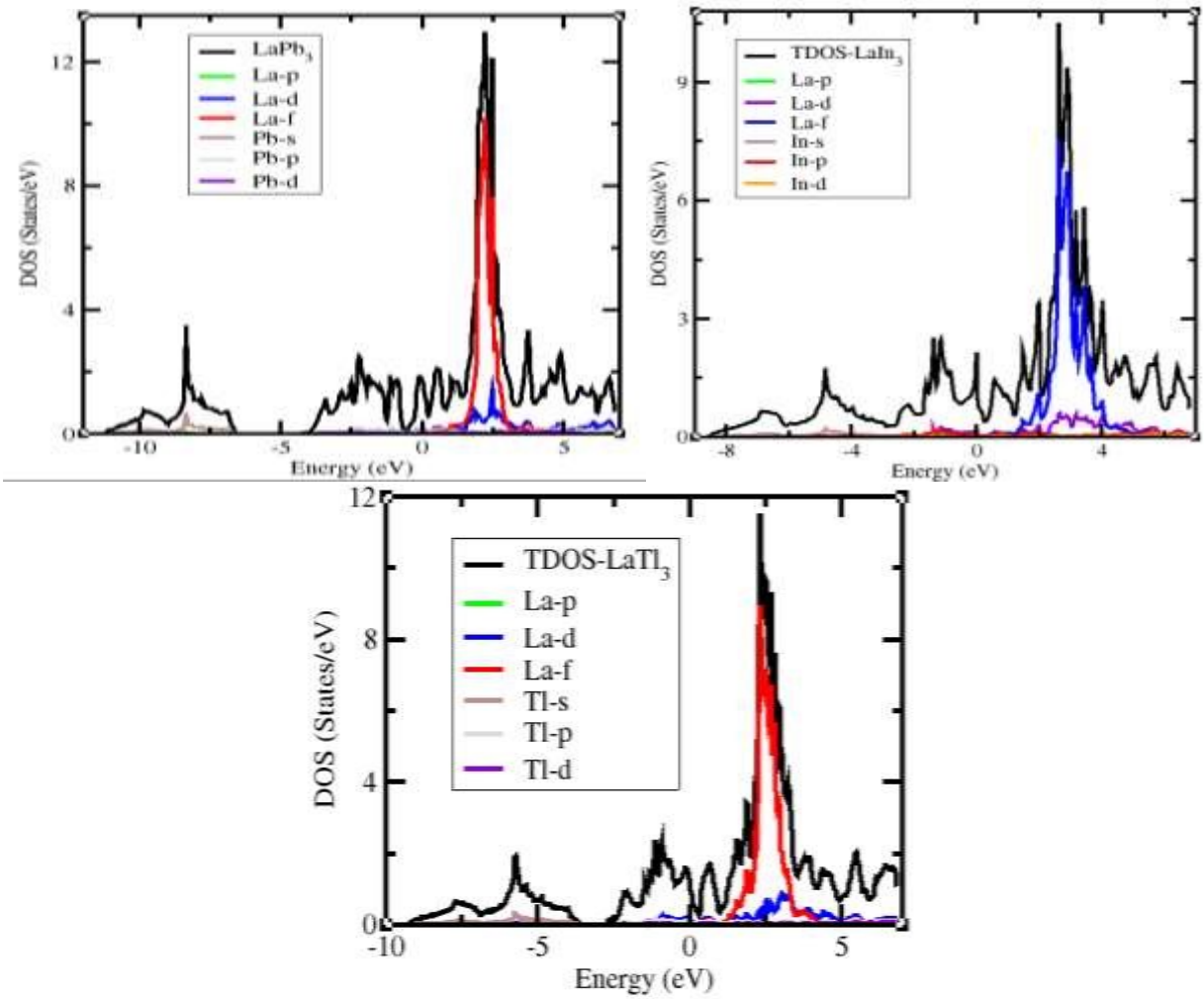

Figure 3.3(a,b,c): TDOS for $LaPb_3$, $LaIn_3$ and $LaTl_3$ by applying B3PW91 hybrid functional. end

3.4 Seebeck Coefficient

A crucial and significant challenge for the long-term advancement of human civilization has always been energy. The conventional energy sources are either on the verge of exhaustion or raise serious environmental issues [34]. To address this pressing issue, researchers are looking for alternate energy sources and energy-saving devices. The thermoelectric energy is one of the significant energy sources. This environmentally friendly technique converts waste heat straight into usable electrical energy. Governments and research organizations have recently given a great deal of attention [35-36]. For thermoelectric devices used in automobiles, residences, and businesses, good thermoelectric materials are necessary [37]. The capacity to convert waste heat into usable electrical energy will be better for materials with a high Seebeck coefficient and high

 DOI 10.69710/ljp.v1i2.11037

figure of merit [38]. Gaining an understanding of the Seebeck coefficient is essential to comprehending the thermoelectric phenomena. The Seebeck Coefficient of a material is used to calculate the amount of Induced Voltage resulting from a temperature differential. The SI unit for the Seebeck Coefficient is volts per Kelvin. The material that creates and cools thermoelectric energy has a significant magnitude value. P-doped materials have a positive Seebeck coefficient [39–42], whereas N-doped materials show a negative value. The ratio of a material's charge carrier concentration to its doping level is known as its chemical potential. Chemical potential is thought to be one of the key elements for enhancing thermoelectric properties [43]. The curve of the Seebeck coefficient vs chemical potential for the rare-earth intermetallic complex LaX_3 (X=Pb, In, Tl) is depicted in Figure 3.4(a,b,c) respectively The figure shows that the highest Seebeck coefficient for the $LaPb_3$, $LaTl_3$ and $LaIn_3$ in the p-type region 38.16 µV/K 57.54 µV/K and 20.23 µV/K respectively. In the n-type region maximum value of Seebeck Coefficient for the same order of compound under study are -44.34 µV/K, -62.75 µV/K and -27.91 µV/K respectively The computations are completed at a temperature of 500 K. The picture makes it obvious that the greatest Seebeck coefficient for the n- and p-type regions in $LaIn_3$, $LaTl_3$ at the chemical potential of 0.002 eV to -0.015 eV for all the compounds under consideration. For all these compounds the n-type area has a higher Seebeck coefficient value than the p-type region. These calculations demonstrate unequivocally that these materials respond more thermoelectrically in the n-type region. The calculations are finished at a 500 K temperature gradient. The image clearly shows that for all the compounds under investigation, $LaIn_3$, $LaTl_3$ has the highest Seebeck coefficient for the n- and p-type regions at the chemical potential of 0.002 eV to -0.015 eV.

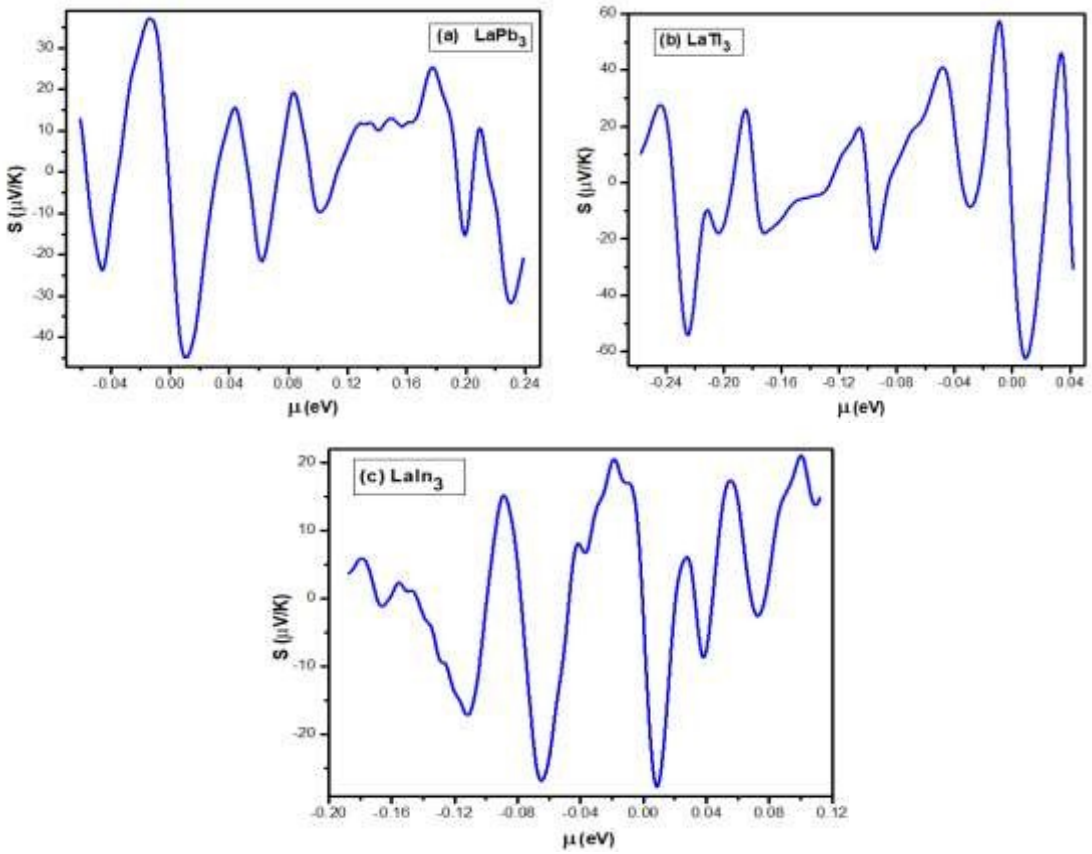

Figure 3.4(a,b,c): Seebeck coefficients for $LaPb_3$, $LaTl_3$ and $LaIn_3$ against the chemical potential.

3.5 Electrical Conductivity

The material's electrical conductivity is used to evaluate its thermoelectric qualities. Both holes and electrons are involved in conductivity. Whereas both holes and electrons participate in conducting current in semiconductors, electrons are the main source of current in conductors [4446]. Figure 3.5(a,b,c) illustrates the relationship between electrical conductivity and chemical potential respectively for the rare-earth

 DOI 10.69710/ljp.v1i2.11037

intermetallic complex LaX_3, where X=Pb, In, and Tl. Electrical conductivity is expressed in these computations in units of order 10^{20} $1/\Omega$ms. In figure σ/τ is maximum for the n-type region for $LaIn_3$. In these calculations n type region maximum value of electrical conductivity for $LaPb_3$, $LaTl_3$ and $LaIn_3$ and are $9.23\times10^{20}1/\Omega$ms, $3.28\times10^{20}1/\Omega$ms and $9.42\times10^{20}1/\Omega$ms respectively. In p-type minimum value of σ/τ for $LaPb_3$, $LaTl_3$ and $LaIn_3$ are $2.42\times10^{20}1/\Omega$ms, $0.41\times10^{20}1/\Omega$ms and $4.10\times10^{20}1/\Omega$ms respectively. Figures demonstrate that electrical conductivity is low for all materials with chemical potentials near to zero and increases when chemical potentials are increased. This implies that we may change chemical potentials to give these materials the desired electrical conductivity values.

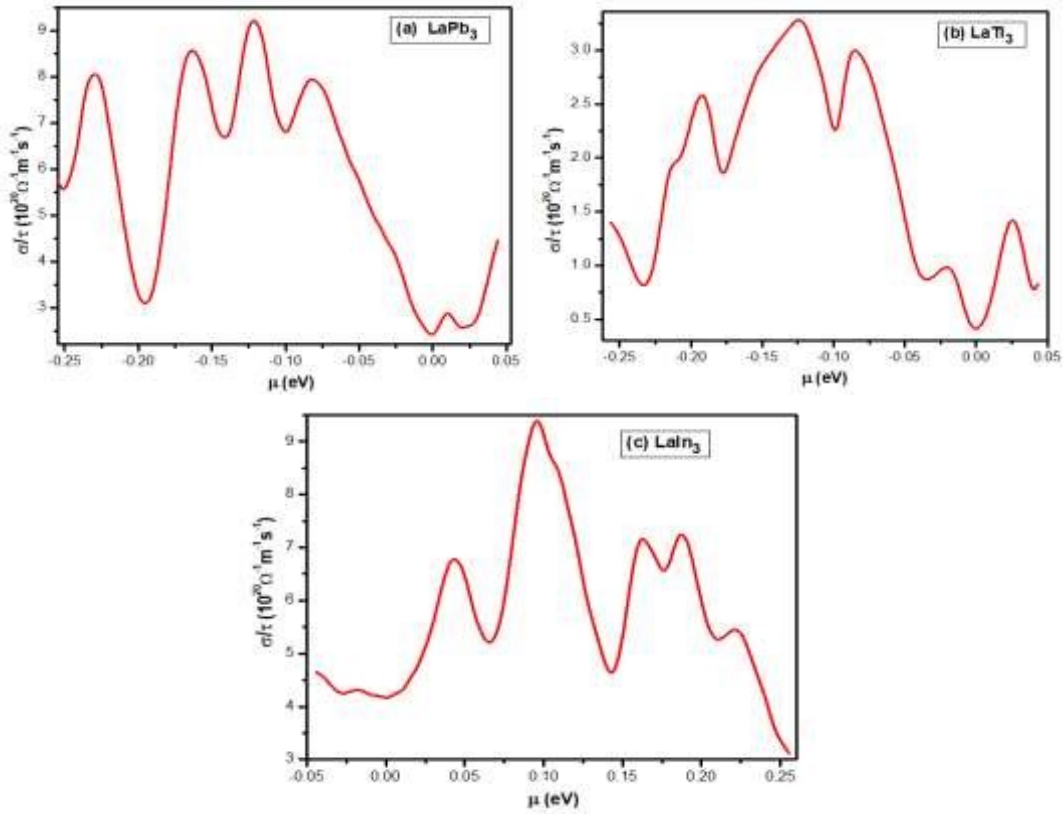

Figure 3.5: Electrical conductivity for $LaPb_3$, $LaTl_3$ and $LaIn_3$ against the chemical potential.

3.6 Electronic Thermal Conductivity per Relaxation Time σ/τ

Thermal conductivity is measured when a temperature gradient is applied through the material. Thermal conductivity in metals is primarily driven by electrons or free charge carriers, but in semiconductors it is attributed to electron-hole pairs [47-50]. The disadvantage of the BoltzTraP code is that the electronic, the thermal conductivity of the heat flow of the material is caused by phononic component of thermal conductance can be determined, but thermal grid cannot be calculated. Figure 3.6(a,b,c) displays the plot of thermal conductivity per relaxation time verses chemical potential for LaX_3 (X=Pb, Tl and In) at 500K temperature gradient. For the compounds under study, the n-type area exhibits a considerable response of thermal conductivity per relaxation time in comparison to the p-type region, the peak value of κ/τ for $LaPb_3$, $LaTl_3$ and $LaIn_3$ in n-type region are 99.46×10^{14}W/mKs, 38.57×10^{14}W/mKs and 107.65×10^{14}W/mKs respectively and in ptype are 29.73×10^{14}W/mKs, 8.11×10^{14}W/mKs and 51.19 $\times10^{14}$W/mKs respectively.

 DOI 10.69710/ljp.v1i2.11037

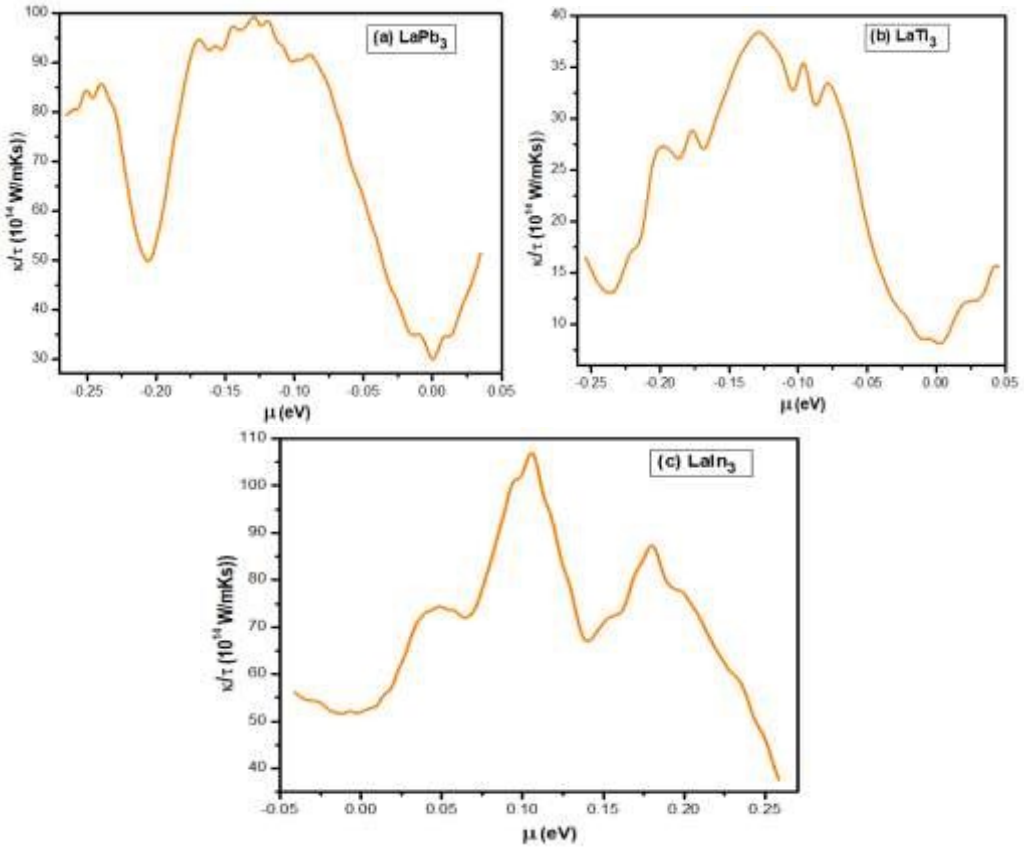

Figure 3.6(a,b,c): Thermal conductivity per relaxation time σ/τ for $LaPb_3$, $LaTl_3$ and $LaIn_3$ against the chemical potential.

3.7 Figure of merit

The figure of merit is a parameter that determines a material's thermoelectric efficiency. The theoretical framework connected with the high Seebeck coefficient specifies the theoretical boundary for studying the yield of thermoelectric materials. Comprehending the figure of merit (ZT) of a material is essential to understanding the productivity of a compound. $ZT = S^2\ \sigma T/\kappa$ is the formula for figure of merit, where S and T are the parameters that are described in terms of the performance of the designated Seebeck coefficient thermoelectric boundary, electrical conductivity and thermal conductivity [51]. Figure 3.7(a,b,c) shows the curve of ZT against chemical potential for the rare-earth LaX_3 (X= Pb, In, Tl) at 500 K temperature gradient. The peak ZT value for each of the compounds under study is depicted as being close to the Fermi level in the picture. This means that n-type doping is a better option for materials with superior thermoelectric capabilities than p-type doping. $LaPb_3$, $LaTl_3$ and $LaIn_3$ each have a peak ZT value in the Figure 3.7(a,b,c) of 0.074, 0.13 and 0.03 respectively. The highest value of figure of merit in spin up calculation is 0.13 for $LaTl_3$. Figure of merit increases with increasing electrical conductivity and Seebeck coefficient while decreases with increasing thermal conductivity.

 DOI 10.69710/ljp.v1i2.11037

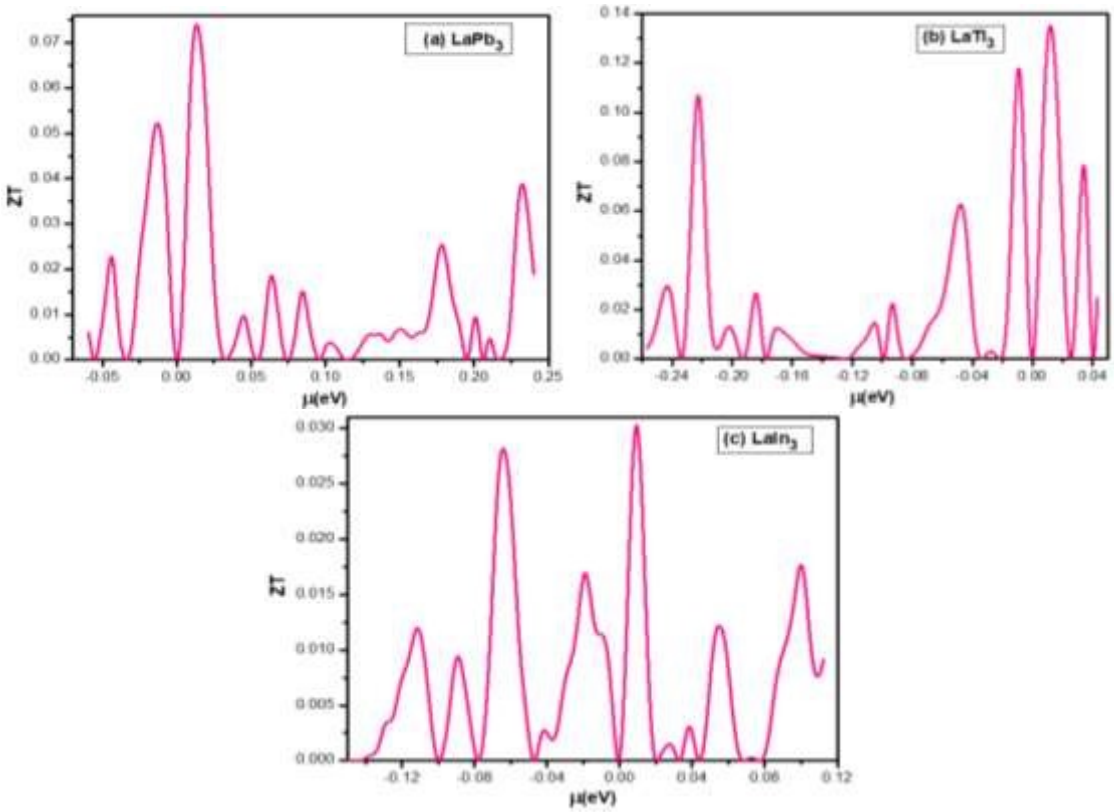

Figure 3.7(a,b,c): Figure of merit (ZT) for $LaPb_3$, $LaTl_3$ and $LaIn_3$ against the chemical potential.

4 Conclusions

Electron charge density indicates that these materials show stronger ionic character. Metallic character of the compound is due to the La, 4f electrons. At the Fermi level, most of the contribution comes from the f state of La, while other states make an almost negligible contribution. For the first time, these materials transport properties have been researched. Highest Seebeck coefficient value for $LaTl_3$ is 57.54 V/K in p-type region. $LaIn_3$ has the highest value of thermal conductivity 107.65×10^{14}W/mKs in the p-type region. $LaTl_3$ has maximum figure of merit (ZT) among these materials which is 0.13, according to the results of the current investigation. When compared to p-type, these materials are more convincing for n-type, due to general implications of transport properties.

5 Funding Information

There was no funding available for this research work.

6 Conflicts of interests

The authors declare that there is no complicit of interest regarding the publication of this paper.

7 Data and code availability

The data and code availability not applicable as no datasets were generated during the current study.

8 Copyright Notice

9 References

[1]. Y. Tokura, and N. Nagaosa, "Orbital physics in transition-metal oxides," *Sci.*, vol. 288, pp. 462- 468, Apr. 2000.

[2]. E. Dagotto, "Complexity in strongly correlated electronic systems," *Sci.*, vol. 309, pp. 257262, Jul. 2005.

[3]. W. Suski, "Physics of the f-electron intermetallics," *Phys. Solid State*, vol. 41, pp. 733-737, May 1999.

[4]. E. Wigner, "On the interaction of electrons in metals," *Phys. Rev.*, vol. 46, pp. 1002-1011, Dec. 1934.

[5]. J. A. Abraham, G. Pagare, S. S. Chouhan, and S. P. Sanyal, "High pressure structural, elastic, mechanical and thermal behavior of LaX_3 (X= In, Sn, Tl and Pb) compounds: A FP-LAPW study," *Comp. Mat. Sci.*, vol. 100, no. 81, pp. 423-432, Jan. 2014.

[6]. R. J. Gambino, N. R. Stemple, and A. M. Toxen, "Superconductivity of lanthanum intermetallic compounds with the Cu_3Au structure," *J. Phys.: Chem. of solids,* vol. 29, no. 2, pp. 295-302, Feb. 1968.

[7]. K. A. Gschneidner, "Physical properties and interrelationships of metallic and semi metallic elements," *Solid State Phys.*, vol. 16, pp. 275-426, Jan. 1964.

[8]. N. V. C. Shekar, and P. C. Sahu, "Pressure induced structural behavior in f-electron based AB, AB_2 and AB_3 intermetallics," *J. Mat. Sci.*, vol. 41, pp. 3207-3228, 2006.

[9]. S. Ram, V. Kanchana, A. Svane, S. B. Dugdale, and N. E. Christensen, "Fermi surface properties of AB_3 (A = Y, La; B = Pb, In, Tl) intermetallic compounds under pressure," *J. Conden. Matter*, vol. 25, pp. 155501(1-9), 2013.

[10]. S. J. Asadabadi, S. Cottenier, H. Akbarzadeh, R. Saki, and M. Rots, "Valency of rare earths in RIn_3 and RSn_3: Ab initio analysis of electric-field gradients," *Phys. Rev. B*, vol. 66, no. 19, pp. 195103- 195113, Nov. 2002.

[11]. K. A. Gschneidner, A. Russell, A. Pecharsky, J. Morris, Z. Zhang, T. Lograsso, D. Hsu, C. H. Chester, Y. Ye, A. Slager, and D. Kesse, "A family of ductile intermetallic compounds," *Nat. Mat.*, vol. 2, no. 9, pp. 587-590, Sep. 2003.

[12]. S. Ram, V. Kanchana, G. Vaitheeswaran, A. Svane, S. B. Dugdale, and N. E. Christensen, "Electronic topological transition in $LaSn_3$ under pressure," *Phys. Rev. B*, vol. 85, pp. 174531 (1- 8), 2012.

[13]. J. O. Choi, J. Y. Kima, C. O. Choi, J. K. Kim, and P. K. Rohatgi, "Effect of rare earth element on microstructure formation and mechanical properties of thin wall ductile iron castings," *Mater. Sci. Eng. A*, vol. 383, pp. 323-333, 2004.

[14]. J. A. Abraham, G. Pagare, and S. P. Sanyal, "Ab-initio calculations of structural, electronic, elastic and mechanical properties of $REIn_3$ and $RETl_3$ (RE= Yb & Lu) intermetallic compounds," *Advans. Phys. Theories Applications*, vol. 45, pp. 66-71, 2015.

[15]. W. Suski, "Physics of the f-electron intermetallics," *Phys. solid state*, vol. 41, no. 5, pp. 733- 737, May 1999.

[16]. S. J. Asadabadi, S. Cottenier, H. Akbarzadeh, R. Saki, and M. Rots, "Valency of rare earths in RIn_3 and RSn_3: Ab initio analysis of electric-field gradients," *Phys. Rev. B*, vol. 38, no. 2, pp. 1284- 1287, March 2002.

[17]. R. Harris, and G. V. Raynor, "Rare earth intermediate phases: I. Phases formed with tin and indium," *J. Less Common Met.*, vol. 1, no. 4, pp. 598-606, Dec. 1965.

[18]. R. J. Gambino, N. R. Stemple, and A. M. Toxen, "Superconductivity of lanthanum intermetallic compounds with the Cu_3Au structure," *J. Phys. Chem. Solids,* vol. 29, pp. 295-302, 1968.

[19]. P. C. Sahu, N. V. C. Shekar, M. Yousuf, and K. G. Rajan, "Implications of a pressure induced phase transition in the search for cubic Ti_3Al," *Phys. Rev. Lett.*, vol. 78, pp. 1054-1057, 1997.

[20]. K. Burke, "Perspective on density functional theory," *The J. Chemical Phys.*, vol.136, no. 15, pp.

150901-150911, 2012

[21]. Ahmad S, Ahmad R, Jalali-Asadabadi S, Ali Z and Ahmad I. First principle studies of electronic and magnetic properties of Lanthanide-Gold (RAu) binary intermetallics. *J. Magn Mater.* 2017, 422: 458.

[22]. J. P. Perdew, J. Chevary, S. Vosko, K. A. Jackson, M. R. Pederson, D. Singh, and C. Fiolhais, "Atoms, molecules, solids, and surfaces: Applications of the generalized gradient approximation for exchange and correlation," *Phys. Rev. B*, vol. 46, no. 11, pp. 6671, 1992.

[23]. H. Hartmann, K. Berggold, S. Jodlauk, I. Klassen, K. Kordonis, T. Fickenscher, R. Poettgen, A. Freimuth, T. Lorenz, "*J. Phys.: Condens. Matter*," vol. 17, p. 7731, 2005.

[24]. A. Reshak and S. A. Khan, "Density of electronic states and dispersion of optical functions of defect chalcopyrite $CdGa_2$ X_4 (X= S, Se): DFT study," *Mater. Res. Bull.*, vol. 48, no. 11, pp. 555, 2013.

[25]. H.R. Aliabad and M. Kheirabadi, "Thermoelectricity and superconductivity in pure and doped Bi2Te_3 with Se," *Physica B: Condensed Matter*, vol. 433, p. 157, 2014.

[26]. G. K. Madsen and D. J. Singh, "BoltzTraP. A code for calculating band-structure dependent quantities," *Comput. Phys. Commun.*, vol. 175, no. 1, p. 67, 2006.

[27]. W. C. Witt, B. W. Shires, C. W. Tan, W. J. Jankowski, and C. J. Pickard, "Random Structure Searching with Orbital-Free Density Functional Theory," *The Journal of Physical Chemistry A*, vol. 125, no. 7, pp. 1650-1660, 2021.

[28]. T. Kaur and M. M. Sinha, "Probing thermoelectric properties of high potential Ca_3PbO: An Ab Initio Study," *IOP Conference Series: Materials Science and Engineering*, vol. 1033, no. 1, p. 012080, IOP Publishing, 2021.

[29]. Z. Ma, X. Wang, and A. Yang, "Influence of temperature on characters of thermoelectric generators based on test bed," *J. Nanomater.*, vol. 2014, no. 3, pp. 1-6, 2014.

[30]. J. P. Perdew, M. Ernzerhof, and K. Burke, "Rationale for mixing exact exchange with density functional approximations," *J. Chem. Phys.,* vol. 105, no. 22, pp. 9982-9985, 1996.

[31]. M. Dipsey, "Working Towards a Normally Off GaN Based MOSHEMT,"

[32]. K. A. Moltved, and K. P. Kepp, "The Metal Hydride Problem of Computational Chemistry: Origins and Consequences," *The Journal of Physical Chemistry A,* vol. 123, no. 13, pp. 2888-2900, 2019.

[33]. Q. X. Xie, J. Wu, and Y. Zhao, "Accurate non-empirical correlation energy functional for uniform electron gas," *arXiv preprint arXiv*:2009. 2689, 2020.

[34]. Z. Ma, X. Wang, and A. Yang, "Influence of temperature on characters of thermoelectric generators based on test bed," *J. Nanomater.,* vol. 2014, no. 3, pp. 1-6, 2014.

[35]. D. Dalafave, "Thermoelectric properties of $Re_6GaxSeyTe_{15}$, *Mater.Chem. Phys.,* vol. 119, no. 1, pp. 195-200, 2010.

[36]. Y. Pei, X. Shi, A. Lalonde, H. Wang, L. Chen, and G. J. Snyder, "Convergence of electronic bands for high performance bulk thermoelectrics," *Nat.*, vol. 473, no. 7345, pp. 66-69, 2011. [37]. P. Ruleova, C. Drasar, P. Lostak, C.-P. Li, S. Ballikaya, and C. Uher, "Thermoelectric properties of Bi_2O_2Se," *Mater. Chem. Phys.*, vol. 119, no. 1, pp. 299-302, 2010.

[38]. X. Qu, W. Wang, W. Liu, Z. Yang, X. Duan, and D. Jia, "Antioxidation and thermoelectric properties of ZnO nanoparticles-coated -$FeSi_2$," *Mater. Chem. Phys.*, vol. 129, no. 1, pp. 331- 336, 2011.

[39]. C. Claeys, P. C. Hsu, Y. Mols, H. Han, H. Bender, E. Seidel, *et al.*, "Electrical activity of extended defects in relaxed InxGa1 xAs Hetero-Epitaxial Layers," *ECS Journal of Solid State Science and Technology,* vol. 9, no. 3, pp. 033001-033017, 2020.

[40]. A. Ikeda, S. Koibuchi, S. Kitao, M. Oudah, S. Yonezawa, M. Seto, and Y. Maeno, "Negative ionic states of tin in the oxide superconductor Sr_3xSnO revealed by Mössbauer spectroscopy," *Physical Review B*, vol. 100, no. 24, pp. 245145-245149, 2019.

[41]. P. Blaha, K. Schwarz, G. Madsen, D. Kvasnicka, and J. Luitz, "WIEN2k, An augmented plane wave plus local orbitals program for calculating crystal properties user's guide," WIEN2k 14.2, Vienna University of Technology, Inst. Physical & Theoretical Chem. Getreidemarkt 9/156, A-1060 Vienna/Austria, 2014.

[42]. M. Saeed, I. Haq, A. Saleemi, S. Rehman, *et al.*, "First-principles prediction of a ground state crystal structure of double perovskite halides Cs_2AgCrX_6 (X = Cl, Br and I)," *Journal of Physics and Chemistry of Solids*, vol. 160, p. 110302, 2022.

[43]. T. Kaur, and M. M. Sinha, "Probing thermoelectric properties of high potential Ca3PbO: An Ab Initio Study," *IOP Conference Series: Materials Science and Engineering*, vol. 1033, no. 1, p. 012080, IOP Publishing, 2021.

[44]. M. Baira, A. B. Siad, and M. B. Siad, "A new investigation of Ruddlesden-Popper compounds Ba_2MO_4 (M= Sn, Pb) through structural, elastic, electronic, optical and thermoelectric properties," *Journal of Solid State Chemistry*, vol. 294, pp. 121843-121850, 2021.

[45]. S. Feng, N. Wang, M. Li, H. Xiao, Z. Liu, X. Zu, and L. Qiao, "The thermal and electrical transport properties of layered LaCuOSe under high pressure, "*Journal of Alloys and Compounds*, vol. 861, pp. 157984-157989, 2021.

[46]. H. Wiebeler, "A linear scaling DFT-Method and high-throughput calculations for p-type transparent semiconductors," Doctoral dissertation, University, 2020.

[47]. J. N. Hausmann, M. Oudah, A. Ikeda, S. Yonezawa, and Y. Maeno, "Controlled synthesis of the ant perovskite oxide superconductor Sr3-xSno,"*Superconductor Science and Technology*, vol. 31, no. 5, pp. 055012-055018, 2018.

[48]. X. Yuan, Y. Sun, H. Guo, K. Shi, P. Song, H. Han, "Design of negative/nearly zero thermal expansion behavior over a wide temperature range by multi-phase composite," *Materials & Design*, vol. 203, pp. 109591-109601, 2021.

[49]. H. Yamamoto, T. Imai, Y. Sakai, and M. Azuma, "Colossal negative thermal expansion in electron-doped ABX tetragonal," *Angewandte Chemie International Edition,* vol. 57, no. 27, pp.

8170-8173, 2018.

[50]. B. G. Janesko, P. Verma, G. Scalmani, M. J. Frisch, and D. G. Truhlar, "M11plus, a rangeseparated hybrid meta functional incorporating nonlocal rung-3.5 correlation, exhibits broad accuracy on diverse databases," *The Journal of Physical Chemistry Letters*, vol. 11, no. 8, pp.

3045-3050, 2020.

[51]. F. Y. Zhang, P. Qin, S. Liu, Q. Yang, J. Meng, and J. Xie, "Characterization of elevatedtemperature high strength and decent thermal conductivity extruded Mg-Er-Y-Zn alloy containing nano-spaced stacking faults," *Materials Characterization*, vol. 155, pp. 109823-109834, 2019.